Aerodynamic forces on railway acoustic barriers

Soper, David; Gillmeier, Steffi; Baker, Christopher; Morgan, Thomas; Vojnovic, Luka

DOI:
10.1016/j.jweia.2019.06.009

Document Version
Peer reviewed version

Citation for published version (Harvard):
Soper, D, Gillmeier, S, Baker, C, Morgan, T & Vojnovic, L 2019, 'Aerodynamic forces on railway acoustic barriers', *Journal of Wind Engineering and Industrial Aerodynamics*, vol. 191, pp. 266-278. https://doi.org/10.1016/j.jweia.2019.06.009

Aerodynamic forces on railway acoustic barriers

David Soper[1], Stefanie Gillmeier[1], Chris Baker[1],
Thomas Morgan[2], Luka Vojnovic[2]
[1] School of Engineering, University of Birmingham,
Edgbaston, Birmingham B15 2TT
[2] UK high speed infrastructure

Abstract

Aerodynamic measurements were conducted to assess the magnitude of pressures measured on a range of acoustic barriers during normal working traffic. A week of measurements were made at a number of tests sites, capturing data for a range of train types. The different test sites allowed for a novel assessment of the influence of barrier distance from centre of track and any influence from other trackside infrastructure. Results exhibited a characteristic pressure development measured on the acoustic barrier, as observed in previous studies, with similar magnitudes recorded for all high speed passenger trains. Pressure magnitudes were largest around the train nose and tail regions. A twelve car train had an additional large peak due to the coupling of two six car sets. As barrier distance from centre of track was increased the magnitude of pressures measured was shown to decrease. Fitting a curve of best fit to the results indicated that the same curve form could be used for both the positive and negative nose pressures. Differences in peak pressure magnitudes were observed for results measured underneath the footbridge suggesting a potential influence of the footbridge on the aerodynamic flow development. CEN standards were shown to offer a good estimation to the pressure coefficient measured on the barrier at most positions analysed. Analysis of peak pressure magnitudes in relation to the number of train passes across the barrier life span, calculated through a rainflow analysis, suggested that small pressure fluctuations were the dominant feature across all measurements. Larger fluctuations depended on train type and as such load calculations should account for the different types of traffic observed on the railway.

Nomenclature

$\mathbf{y}$	unit vectors associated with axes Y	E_{TOT}	Total error
ρ	Air density (kg/m^3)	F_Y	Load force (N)
τ	Normalised time scale	k	Individual pressure transducer
A_{ij}	Area ij (m^2)	p_0	ambient pressure (Pa)
A_{ref}	Reference area (m^2)	V_{train}	train speed (m/s)
b_k	Individual quantity in error calculation	x	distance measured from vehicle nose along the track (m)
$C_{P_{2\sigma}}$	Ensemble coefficient of pressure plus two standard deviations	y	distance measured normal to the track from the centre of track (m)
C_P	Coefficient of pressure	z	distance measured from the top of the rail in the vertical direction (m)
C_Y	Force coefficient		
E_{BIAS}	Uncertainty of a measured variable due to instrumentation accuracy	n_{ij}	normal unit vector associated with discretised area A_{ij}

1 Introduction

A railway in the simplest form is a trackbed earthwork onto which a set of railway tracks are laid, on which a train can run. The railway system as a whole however is a much more complex set of infrastructure built around this simple form, taking into account the needs of a modern railway network and adapting to the surroundings through which the railway is passing. Examples of this infrastructure include footbridges, overhead line equipment, signalling equipment and acoustic barriers. Acoustic barriers are essentially a series of large screens built parallel to the railway to provide a level of acoustic and visual screening from the railway and a level of security.

As a train moves it forces the air around the vehicle out of the way, creating a complex aerodynamic flow with a highly turbulent boundary layer development and extensive wake flow. The aerodynamic flow around a moving train interacts with the different trackside infrastructure through which the train is passing, imparting a dynamic pressure load signal into the structure. The majority of all modern trackside infrastructure is designed to withstand the magnitude, frequency and number of pressure loads exerted

into the structure within a 20 year no maintenance period [2]. Indeed, all new railway vehicles should adhere to a set of standards on railway aerodynamics, given as a predefined limit on pressure magnitudes measured on a trackside structure at a certain distance from centre of track [5, 7, 6].

The introduction of dedicated high speed railway lines around the world has led to issues associated with running trains at very high speeds, such as infrastructure development, train design and maintenance. In countries such as South Korea and China, train speeds have steadily increased over time and the infrastructure is now capable of coping with train speeds approaching 400 kph. Aerodynamic effects increase approximately proportionally with air speed squared, consequently at higher speeds aerodynamic effects will be significantly greater than for trains travelling at lower speeds. In recent years there have been a number of failures of trackside infrastructure, namely acoustic barriers in Germany, which have been exacerbated by aerodynamic effects [8, 4, 14].

One of the major issues cited in relation to the failed acoustic barriers was that structures were designed before the dedicated CEN railway aerodynamic standards were available and as such structures were designed in relation to local railway or even highways standards which may not be suitable for high speed railway lines [2]. Indeed, recent failures of highway acoustic barriers in China have observed similar failure type behaviour through structure deformation and cracking in the structure mounting points [16]. Results from experimental campaigns revealed vehicle induced aerodynamic loads cause alternating stress on structures which could lead to fatigue problems given the frequency of traffic and different types of vehicle cross-section [16, 9].

Work has also been undertaken to analytically model the pressure effects

due to a passing vehicle on a road/trackside structure. The application of potential flow theory in a one dimensional analysis has been shown to provide representative results when compared to experimental data [11, 12, 15, 8]. An analytical approach is also adopted in the CEN railway aerodynamic standards to estimate the maximum and minimum peak pressure magnitudes for a given train type and structure distance from centre of track [6, 8].

This study presents a novel series of aerodynamic measurements undertaken by the University of Birmingham to assess the magnitude of pressures measured on a range of acoustic barriers during normal working traffic. The measurements were made to analyse the effects of high speed passenger train aerodynamics on acoustic barriers, to support the knowledge base of structures located on the high speed infrastructure. A week of measurements were made at a number of tests sites along the railway, as discussed in section 2.1. The train types recorded and experiment methodology are presented in section 2. The techniques and methodology for analysing the data are discussed in section 3. A discussion of experimental uncertainty is presented in section 4. An overview of the characteristic pressure development is given in section 5.1. This is expanded to discuss influencing factors on peak pressure magnitudes, sections 5.3 to 5.5. Peak pressure results are compared to values calculated using the CEN standards methodology, section 5.4, and an estimate to the load force measured on the acoustic barrier is made, were possible, in section 5.6. Finally, an analysis of fatigue loads is made by assessing the magnitude and frequency of dynamic pressure loads experienced by the acoustic barriers, given in section 5.7. The analysis is expanded to include for the first time a rainflow type analysis of pressure fluctuations, assessing how fluctuations relate to the types of barriers and

trains analysed.

2 Experiment methodology

2.1 Test sites

Two test sites were chosen based on the distance of the acoustic barrier from the centre of track (COT) and the barrier construction method. The acoustic barrier at site 1 is identified as the white line in the aerial view shown in figure 1 and photographs of the site are shown in 2. At site 1 there are two lines (max speed 63.33 m/s for high speed passenger trains). Acoustic barriers are positioned on both sides of the site; however, the positioning is staggered and as such no barrier was positioned across from the measuring sites. A small path separates the edge of the track, effectively marked by the overhead line stanchions and the base of the acoustic barrier. The rear side of the acoustic barrier is relatively constrained, marked by a small footpath and a large storm drain on the other side (figure 2). Specialist scaffold equipment was erected to enable the measuring instrumentation to be installed across the full height of the barrier. A number of positions were tested at site 1 based on different barrier sections at distances 3.72 m, 4.19 m, 4.68 m and 5.04 m from centre of track.

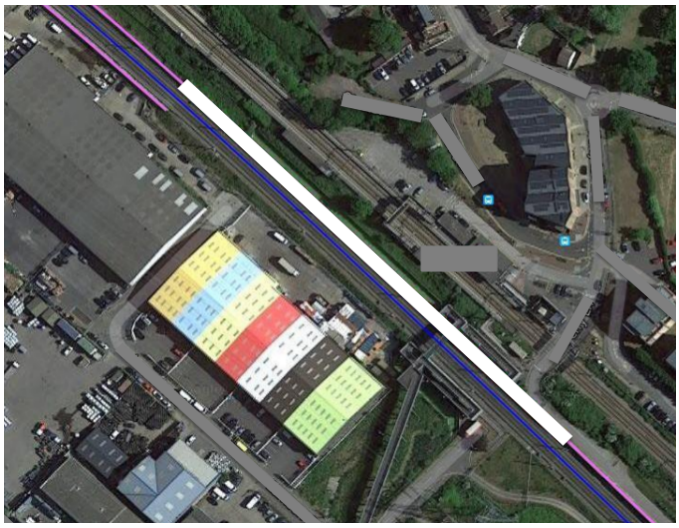

Figure 1: An aerial view of experiment site 1. The acoustic barrier is shown as the white line. Image from GIS model of the route.

(a) Absorptive trackside view

(b) Reflective trackside view

(c) Rear side view

Figure 2: The acoustic barrier at experiment site 1.

The barrier at site 1 has two types of construction. The first is an absorptive type barrier consisting of a thin perforated metal sheet, an air gap, and a layer of rock wool insulation attached onto a thick wooden backing (figure 2(a)). The barrier has a sheet metal top. The barrier is constructed in bay sections marked by a series of vertical metal RSJ type columns which are bolted to a specialist concrete pad, mounted on a large concrete slab onto which the railway is laid. The second barrier type is the reflective barrier which is essentially the same type of barrier but with the thin perforated metal sheet, rock wool and sheet metal top removed; i.e. a series of vertical metal RSJ type columns with a thick wooden backing (figure 2(b)).

Test site 2 acoustic barrier is identified as the white line in the map shown in figure 3. The location was selected as the acoustic barrier is of slightly different construction to site 1; it is further away from the centre of track (5.17 m) and has a section underneath a footbridge. The current studies will investigate whether the footbridge influences the magnitude of aerodynamic forces on the barrier. At the test site there are two lines (max speed 75 m/s for high speed passenger trains), with an acoustic barrier only positioned on one side of the railway. The barrier itself is however situated in a small cutting and as such the test site itself was relatively constrained due to the cutting slope and the railway, figure 4. The barrier construction at site 2 is the same as the site 1 barrier, an absorptive type; however, the vertical metal RSJ type support columns are set into concrete blocks buried into the ground rather than mounted to a concrete slab.

Figure 3: An aerial view of experiment site 2. The acoustic barrier is shown as the white line. Image from GIS model of the route.

(a) Trackside view (b) Rear side view

Figure 4: Experiment site 2 acoustic barrier.

2.2 Train types

This paper will analyse a cross section of the rail traffic that runs on the infrastructure. Table 1 gives an overview of the characteristic details of each train.

	Train type			
	Train 1	Train 2	Train 3	Train 4
Maximum permitted train speed (m/s)	83.67	83.67	62.59	40
Train length (m)	394	400	121.3 or 242.6	500
Number of carriages	20	16	6 or 12	20

Table 1: Types of trains analysed.

2.3 Aerodynamic instrumentation

Small instrumented units housed in an IP67 box were fixed to the rear side the acoustic barrier at 1 m intervals in increasing height above the ground,

starting from height 0.5 m. The pressure measuring instrumentation was placed inside the barrier via a hole drilled in the wooden back panels of the wall. Each instrumented unit contained two differential pressure transducers. The instrumented units were connected to a Campbell Scientific CR9000X data logger positioned on the ground beneath the acoustic barrier via an electrical cable and pneumatic tubing. Additional static pressure sensors were also mounted to the acoustic barrier, via cable ties, to assess an alternative method of measuring pressure magnitudes. The general equipment layout is shown in figure 5. The following sections will provide more detail on the individual components of the experiment.

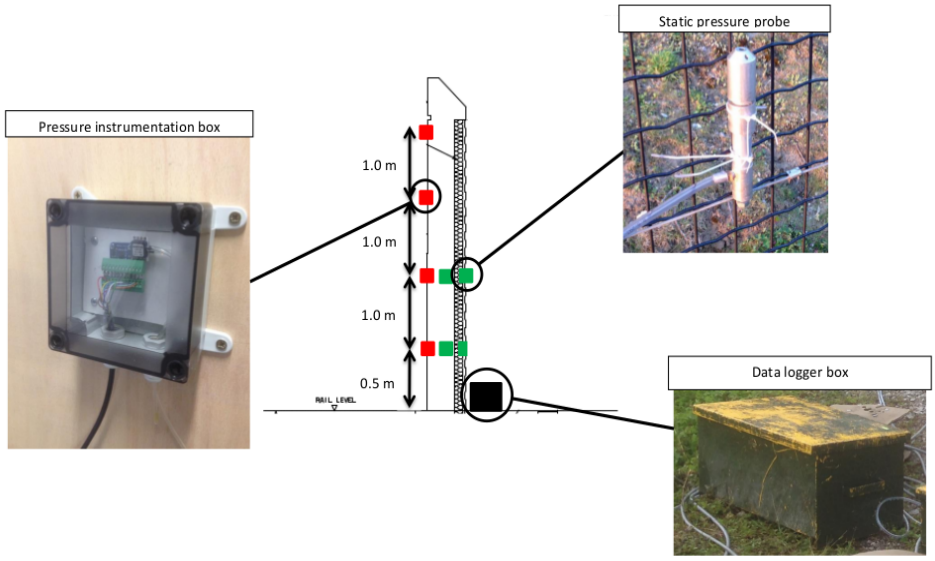

Figure 5: General arrangement of measuring instrumentation.

2.3.1 Static pressure

Static pressure on the acoustic barrier was measured by FirstSensor HCLA12X5 differential pressure transducers. The pressure transducers have two pressure ports to measure the difference in pressure between a measurement

port and a reference port. The measurement port was connected to a small section of pneumatic tube that was fed from the instrumented box through a hole cut in the wooden rear panel to a perforated hole on the front panel of the acoustic barrier, fitting flush with the barrier surface. The reference port was connected to a longer section of pneumatic tube that was fed from the instrumented box to a manifold. The manifold was connected to all pressure transducer reference ports, then connected to a larger diameter pneumatic tube that was fed away behind the acoustic barrier and fixed to the scaffold in a sheltered position away from the influence of passing trains or ambient winds. All pressure transducers were calibrated using a Betz 2500 micro-manometer and a resonant frequency test was performed to correct for any distortion of measured pressures due to the tubing lengths.

Static pressure was also measured on the acoustic barrier surface by a series of static pressure probes. The probes were designed by Moran and Hoxey [10] as a method of easily measuring the static pressure on the surface of a building without the need of creating a pressure tap. The probes were mounted inside the acoustic barrier and on the track side of the front panel by cable ties. The static pressure probes were connected via pneumatic tubing to a differential pressure transducer via the same method as the pressure tap.

2.3.2 Position finders

Mounted to the acoustic barrier either side of the measuring site were further static pressure probes. These probes were set up at a known distance apart and used to measure the train speed of passing trains in relation to the static pressure pulses. The position finder data was also used as a method to align data during the processing stage. The probe was set up using the

same method as section 2.3.1.

2.3.3 Ambient condition monitors

Ambient wind speed measurements were made at site 1 using a Gill type 50 Hz ultrasonic anemometer (USA) set up behind the acoustic barrier in a position away from the influence of passing trains and open enough to measure ambient winds. The anemometer was capable of measuring 3-components of velocity and the mean flow direction at a sampling frequency of 50 Hz. The anemometer was mounted via scaffold fixings to a section of scaffold on the far side of the open storm drain. This measuring position was not ideal and findings will be discussed in section 4. The USA was connected via a long cable to an interface unit that plugs directly into the Campbell Scientific CR9000X data logger unit positioned at the base of the acoustic barrier. It was not possible to measure ambient winds at test site 2 due to the positioning of the barrier in a cutting surrounded by woodland. Analysis of local weather station information indicated localised wind speeds in the area of the test were minimal throughout the test period.

3 Analysis methodology

Data was collected for all instrumentation continuously over a 5 day period for each measuring site, creating a series of large data sets. Initially the large data set was split into a series of files for each individual train pass by cross referencing against the Real Time Trains (RTT) database. The RTT data was used to split the large data sets into a series of 60 second files centred about each train pass. Once split into individual train passages and train type, data was processed with respect to two cut-off values. CEN standards suggest that aerodynamic measurements should be made in ambient wind

conditions below 2 m/s and train speeds should lie within ±5% of the maximum permitted train speed for individual vehicle types [6]. By adopting these limits it was found that the majority of ambient wind speeds measured were below 2 m/s. Train speeds at both sites were shown to be fairly stable throughout the test periods and close to the maximum line speeds of 63.33 m/s and 75 m/s for site 1 and 2 respectively.

To assess the loads on a structure it is important to analyse regions of large pressure fluctuation; these are observed as the nose and tail of a train passes the instrumentation. All data was aligned so that the origin occurs when either the train nose or the train tail passed the measuring instrumentation, taken to be the positive or negative pressure peak respectively. The region over which the analysis is undertaken is relatively short, and as train speeds lie within CEN standards of ±5% it was not necessary to resample the data to remove the effects of changing train speed past the measuring site. Data is however normalised with respect to the individual train speed from each run to allow data from each individual run to be analysed with respect to other runs and ensemble averages created. Ensemble results presented are normalised with respect to train speed to allow the reader to compare different train types easily,

$$C_P(\tau) = \frac{p(\tau) - p_0}{\frac{1}{2}\rho V_{train}^2} \tag{1}$$

where τ is a normalised time scale, in relation to the individual nominal train speed V_{train} and train length depending on train type, such that $\tau = 0$ is the train nose and $\tau = 1$ is the train end. The coefficient of pressure C_P is calculated with respect to an ambient reference pressure p_0 and the air density ρ. The ambient reference pressure was situated beneath the

scaffold away from the influence of passing trains and air density was taken as constant $\rho = 1.225$ kg/m^3.

To analyse the results, data from individual runs was averaged for each measuring position using ensemble averaging techniques. CEN standards [6] state that 10 independent runs should be measured to form an ensemble average of pressure data. In most cases 10 independent runs were available to make the ensemble average; however, when further runs were available these were also included to increase the stability of the ensemble. Table 2 shows the number of runs for each train type analysed at each test site examined.

Distance from COT (m)	Train 1	Train 2	Train 3 (6 car)	Train 3 (12 car)	Train 4
3.72 m Absorp (site 1)	22	22	169	25	3
4.19 m Reflect (site 1)	11	25	53	17	2
4.68 m Absorp (site 1)	5	8	21	9	7
5.04 m Absorp (site 1)	5	8	21	9	7
5.17 m Absorp (site 2)	14	41	81	24	1

Table 2: Ensemble sizes for each train type at each experiment site.

4 Error analysis

An uncertainty analysis methodology is applied to the maximum and minimum pressure values for the head pressure pulse to provide an estimate to uncertainty of recorded data. The experimental data can be considered as a non-dimensional coefficient, calculated using a series of measured variables; such as temperature, ambient pressure, air density and train speed, as discussed above. To account for the combined influence of individual uncertainties associated with each variable, the theory of propagation of error is applied to calculate the coefficient uncertainty. Total uncertainty is defined as the sum of random uncertainties and the uncertainty of a measured variable due to instrumentation accuracy. The uncertainty calculations indicate that the mean uncertainty associated with the measuring instrumentation for each experiment is of the order of $\pm 1 - 2\%$, whereas following the data correction with respect to nominal values the random error decreases to $\pm 1\%$. Therefore the overall estimated uncertainty associated with the data is of the order $\pm$2-3%.

The values provide an estimate of the uncertainties of measured data. The uncertainties are considered to be estimations to the true error, as the methodology does not take into account changes in train speed through the measuring site or fluctuations in ambient conditions. As discussed, the reference anemometer position at site 1 was not ideal for making ambient wind measurements, due to the confinement of the site and no measurements could be made at site 2. Application of CEN standard limits on ambient wind speeds when analysing the data reduces the influence of ambient wind speeds but does not take into account wind direction. However, analysis of data from individual runs indicated little run-to-run difference for all runs analysed, and as such any influence from ambient winds is considered

minimal for this experiment.

5 Results

Initially, an overview of the typical pressure development measured on the barrier when a train passes is discussed. This is then expanded to visualise the key peak-to-peak regions around the train nose and tail, analysing the effect of individual runs against the ensemble average. Results are compared to the methodology presented in the CEN standards to estimate pressure magnitudes on trackside structures. Finally, by integrating peak pressure results over the height of barrier the load on the barrier is estimated.

5.1 General flow development

Figure 6 shows the pressure development on the site 1 acoustic barrier for Train 1. It is clear to see a large characteristic positive then negative peak created as the train nose passes the measuring site. A series of minor pressure transients are created along the train length due to the gaps at the inter-carriage spacing. A larger inter-carriage peak is seen at the centre of the train, related to a larger gap between Train 1 carriages at this point. The characteristic pressure change observed at the train tail has the negative peak first, rising to a positive peak; however, the magnitude of the tail peaks are much lower than the nose peaks. The pressure trace follows the typical trend of development for a high speed passenger train with peak magnitudes similar to values measured in previous studies [3].

Figure 7 illustrates the run-to-run variability of the pressure results in relation to the ensemble mean for Train 1. Pressures measured on trackside structures are in general more repeatable than slipstream velocities, as such only a small number of runs are required to create a stable ensemble average.

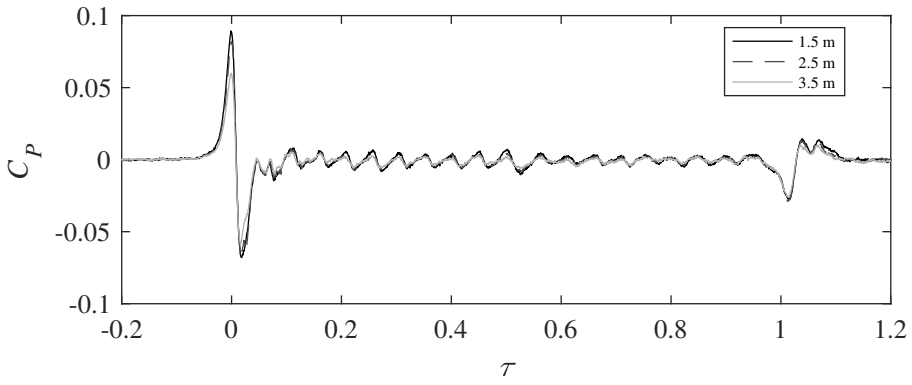

Figure 6: Ensemble pressure development on the barrier due to the passage of Train 1.

This is important as it reduces the uncertainty of the results measured, thus reducing the error calculation (as discussed in section 4). Results indicate good repeatability for all train types examined giving confidence that the ensembles averages created are representative of the pressure development on the acoustic barrier. The additional pressure transient following the negative peak is thought to be related to a geometrical feature of the train at this measuring height, as it is not observed for other measuring heights.

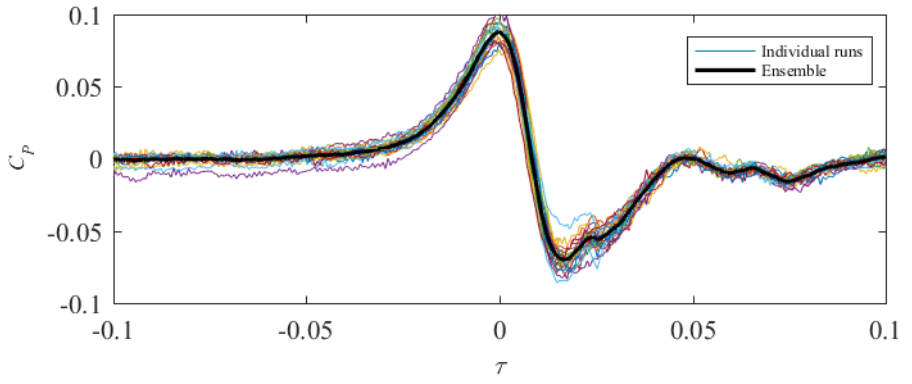

Figure 7: Individual runs and the ensemble for Train 1 at measuring height 2.5 m at site 1.

Expanding the pressure trace to focus on the nose region for all the train types reveals the effect of increasing the measuring height up the barrier (figure 8). Measurements made at the bogie and mid-body height of the train have greater magnitude than measurements made around the train roof, due to the confinement of the flow between the barrier. The normalised peak-to-peak results are similar to those recorded for other aerodynamically smoothed passenger trains [3]. Lachinger et al. [8] also measured peak-to-peak pressures on noise barriers for passing high speed trains. The total peak pressure magnitudes measured agree well with results presented in figure 8 [8].

The characteristic peak-to-peak changes occur for a time base of approximately 0.1 seconds, relating to a distance of 7 m, which corresponds to the length of the aerodynamically shaped nose of the Train 1. Similar values are obtained for Train 2 and Train 3. An additional pressure transient is observed directly after the negative peak for Train 1 and 2 at measuring height 2.5 m on the site 1 barrier. Due to the raised railway bed at this site it is hypothesised that the additional change in pressure (shown clearly in figure 7) is caused by the bogie cut out in the nose region. This feature is not seen for increased distances from centre of track (section 5.3).

Table 3 shows the maximum and minimum ensemble peak values measured in the nose and tail region for each train, as well as the standard deviation (SD) for each value, calculated from the individual runs recorded at site 1. It is clear to see that all results lie relatively close together for Train 1, 2 and 3 with low values of standard deviation. Train 3 exhibits slightly lower peak magnitudes in comparison to Train 1 and Train 2, with differences beyond values of experimental uncertainty. Peak values are similar to values measured in previous studies. Train 4 peak magnitudes are

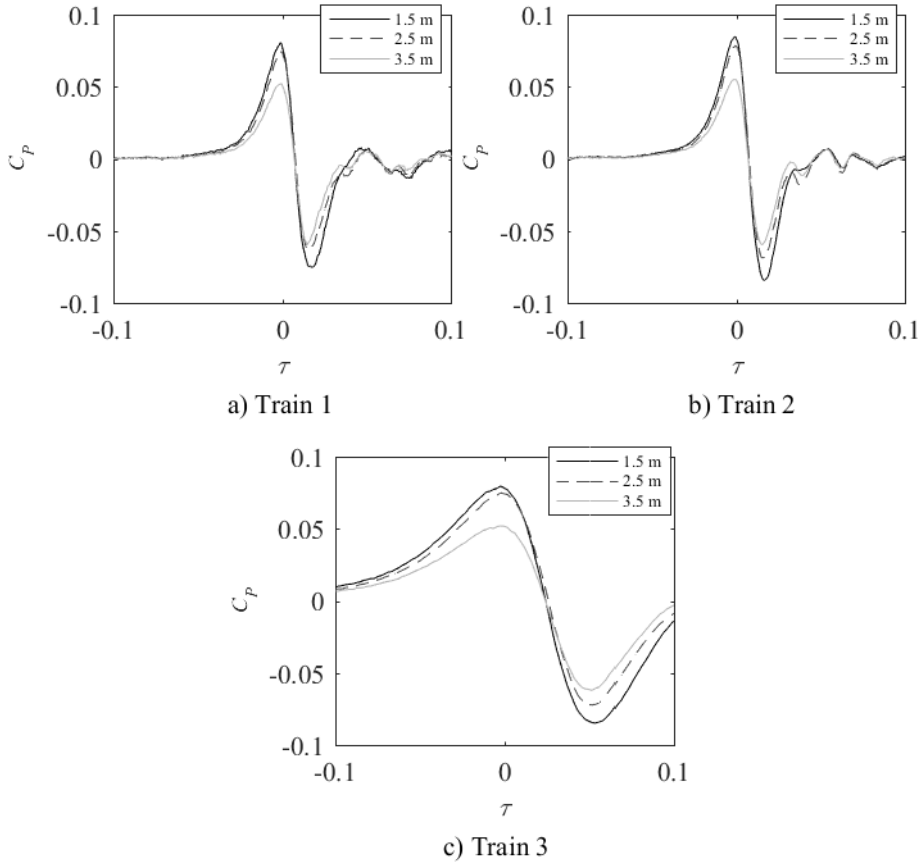

Figure 8: Nose pressure development on the site 1 barrier at each measuring height for each train analysed.

larger than other train values, expected to be due a bluffer train shape in general; however, it should be noted that Train 4 speeds are lower than other train speeds and as such the actual pressure measured is lower than that of the other train.

	Train 1		Train 2		Train 3		Train 4	
Nose	Ensemble	SD	Ensemble	SD	Ensemble	SD	Ensemble	SD
Maximum	0.088	0.007	0.090	0.008	0.084	0.007	0.111	0.009
Minimum	-0.070	0.006	-0.076	0.008	-0.077	0.006	-0.132	0.004
Tail	Ensemble	SD	Ensemble	SD	Ensemble	SD	Ensemble	SD
Maximum	0.015	0.004	0.022	0.005	0.026	0.006	0.044	0.044
Minimum	-0.035	0.005	-0.033	0.006	-0.048	0.007	-0.036	0.033

Table 3: Maximum and minimum ensemble peak C_P values and standard deviations for each train type analysed at measuring height 2.5 m.

A feature of Train 3 is the ability to run in either a 6 or 12 car configuration. The 12 car train consists of two sets of 6 cars joined in the middle, creating a V-shaped region in middle due to the tail and nose of the coupled sets. Figure 9 shows the ensemble pressure trace for the 6 and 12 car trains. It is clear that the V-shaped region creates a further characteristic change in pressure. The magnitude of the positive peak is similar to the tail region; however, the negative peak is much smaller.

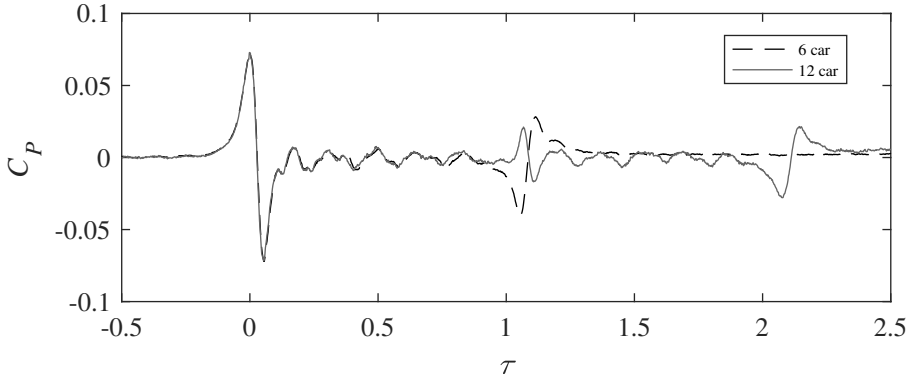

Figure 9: A comparison of Train 3 in a 6 and 12 car configuration.

5.2 Influence of barrier type

Results exhibit similar flow development for both the absorptive and reflective type barriers. The largest peak pressure magnitudes are observed in the train nose region, as such the results presented will focus on this region. Figure 10 shows the Train 2 nose pressures measured for the absorptive and reflective configuration at the same barrier position for increasing measuring heights. It should be noted that for the absorptive configuration no measurement was made at height 0.5 m due to difficulties in the experiment set up. Measurements made at the bogie and mid-body height of the train have greater magnitude than measurements made around the train roof, due to the confinement of the flow between the barrier and train side. Comparison of maximum and minimum peaks for both barrier configurations indicates little difference in peak pressure magnitude; this result is similar for all train types examined. The reflective configuration has slightly lower peak magnitudes, which could be due to the slightly increased distance of 0.47 m away from centre of track, as shown in figure 11 (see section 5.3 for a detailed discussion on the influence of barrier distance from centre of track). Increases of a similar size recorded for other barriers during these test indicated similar magnitude changes in peak pressures, section 5.3. Due to the similarities in findings, the results presented in the rest of the paper will focus on the absorptive barrier type.

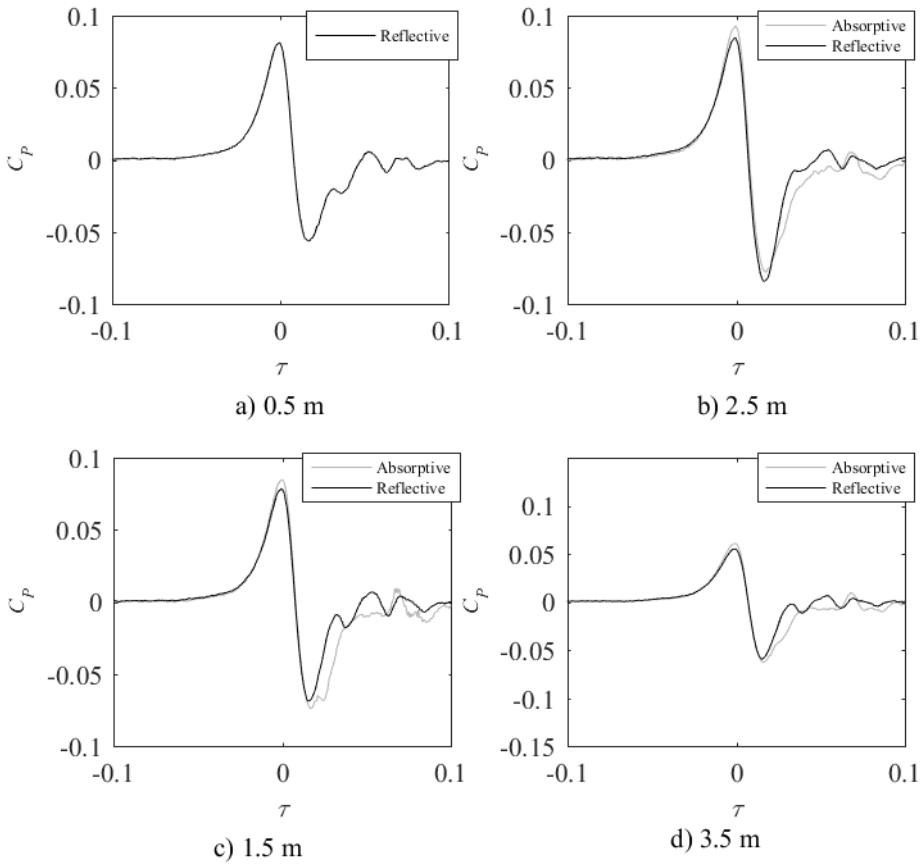

Figure 10: A comparison of nose pressure development for the absorptive and reflective barrier configurations at each measuring height for Train 2.

Figure 11: Difference in position from centre of track between the absorptive and reflective barriers.

5.3 Influence of barrier distance from centre of track

A feature of the acoustic barriers measured was that the positioning in relation to the centre of track for each test site was different. Figure 12 shows the nose pressure magnitudes for Trains 1, 2 and 3 for measurements from sites 1 and 2. It should be noted that the bulk of measurements made at site 1 and 2 were made at height 2.5 m, whereas the final site 1 test was measured at height 2 m. Results across a range of measuring heights, shown in section 5.1, indicated little difference between measurements made at 1.5 m and 2.5 m, and thus it is felt that results from the measuring height of 2 m can be compared with previous results at height 2.5 m. It is clear that as the barrier distance from centre of track is increased the magnitude of peak pressures measured on the barrier surface decreases. This is to be expected and ties in with the numerical methodologies presented in the CEN standards [6].

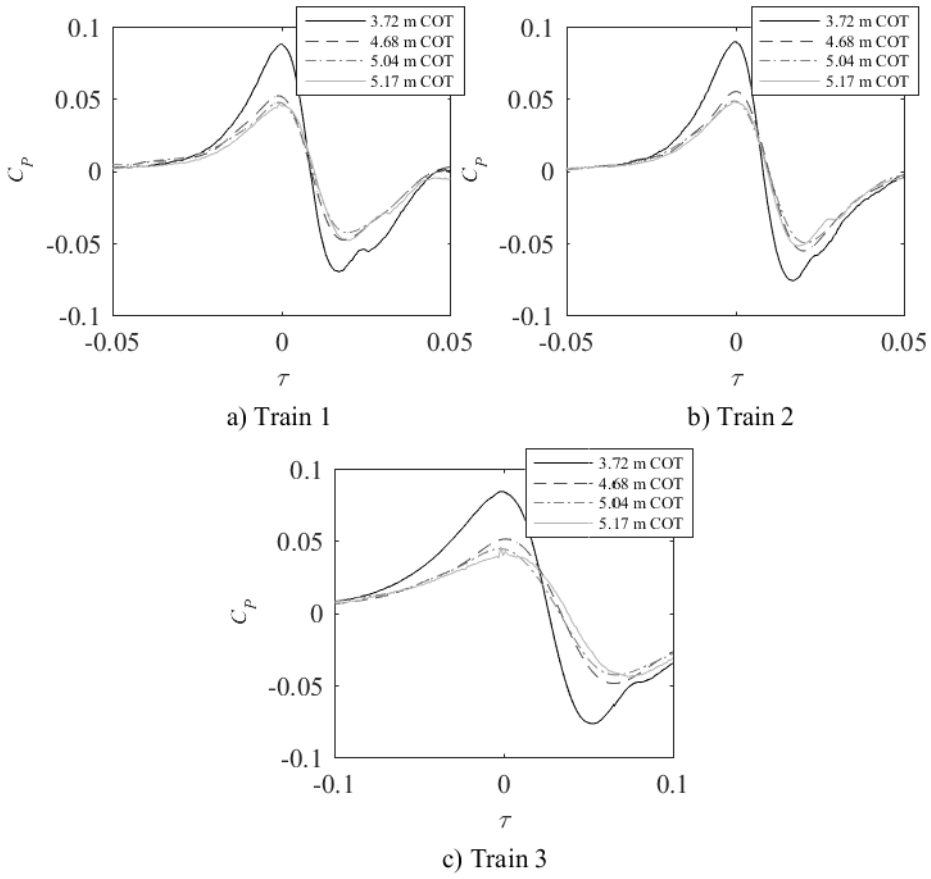

Figure 12: Nose pressure development on the barrier for each train type at all measuring sites for barriers at increasing distances from centre of track.

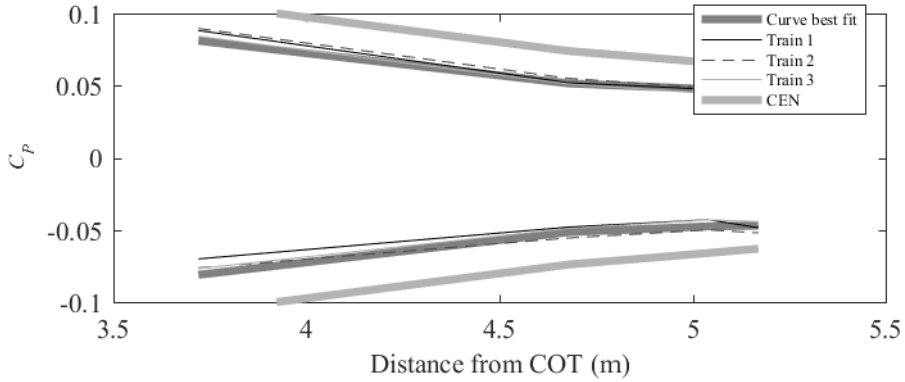

Figure 13: Peak pressure magnitudes in relation to distance from centre of track.

Figure 13 shows the relation between peak pressure magnitudes and the barrier distance from centre of track. Results for all train types are very similar and indicate a comparable relationship which could be used for designing barriers in the future. Fitting a curve of best fit to the results suggests that a second order polynomial relationship is the best fit and that the same coefficient values can be used for both the positive and negative magnitudes for the high speed passenger trains analysed, as shown in equation 3.

$$C_P(y) = 0.015y^2 - 0.156y + 0.454 \tag{2}$$

$$C_P(y) = -0.015y^2 + 0.156y - 0.454 \tag{3}$$

Figure 13 also shows the estimated curve of best fit calculated using the equations given in the CEN standards, discussed in detail in section 5.4. Results suggest that the ensemble peak pressure values sit well within the CEN calculation.

5.4 Comparison with standard methodologies

Requirements on railway aerodynamics are given in a series of CEN standards. In particular 'BS EN 14067-4:2013 Railway applications - Aerodynamics Part 4: Requirements and test procedures for aerodynamics on open track' presents methodologies for assessing pressure loads on vertical structures next to a railway track [6]. The methodology states that pressure peaks in the train nose region are generally largest in magnitude, and that either experimental or computational studies should be conducted to understand peak values for specific structures. A numerical methodology is also presented to estimate the peak pressure magnitudes, based on findings from previous research in this field.

Peak pressure coefficients are estimated through applying the methodology presented in the CEN standard [6] and compared with results measured in this study, shown in table 4. It should be noted that the 'shape coefficient of the train' was taken to be that of a high speed passenger train rather than a standard passenger train, although the actual train speeds past site 1 are lower than the 69.4 m/s cut off. The choice of coefficient was based on the aerodynamically smoothed nature of Trains 1, 2 and 3. The experimental data is presented as,

$$C_{P_{2\sigma}} = \text{ensemble} + 2(\text{SD}) \tag{4}$$

where the ensemble and standard deviation (SD) are as defined in table 3.

Table 4 shows that all experimental data lies below the numerical estimation for the site 1 results. Site 2 results indicate that the positive peak lies below the numerical estimation; however the numerical estimation for the negative peak magnitude is exceeded at numerous measuring positions

	CEN	Experimental		
	High speed passenger train	Train 1	Train 2	Train 3
Site 1 3.72 m COT	$C_{P_{num}}$	$C_{P_{2\sigma}}$	$C_{P_{2\sigma}}$	$C_{P_{2\sigma}}$
Maximum Minimum	0.107 -0.107	0.102 -0.082	0.106 -0.092	0.098 -0.089
Site 1 4.68 m COT				
Maximum Minimum	0.074 -0.074	0.060 -0.057	0.071 -0.069	0.074 -0.070
Site 1 5.04 m COT				
Maximum Minimum	0.066 -0.066	0.054 -0.052	0.064 -0.061	0.063 -0.057
Site 2 5.17 m COT				
Maximum Minimum	0.063 -0.063	0.061 -0.069	0.063 -0.073	0.076 -0.065

Table 4: Comparison of experimental data with the CEN standards numerical estimation.

in the experimental data. In general, for all sites analysed the positive peak is a closer fit than the negative peak which is slightly underestimated.

5.5 Influence of other trackside structures

Site 2 pressure traces are analysed to reveal any effects of the footbridge on the flow development (figure 14). It is clear that the positive pressure peaks for each measuring position are very similar in magnitude, but that the negative pressure peaks exhibit small differences which potentially may be related to the influence of the footbridge positioning. Analysing peak pressure values indicated that all ensemble peak results measured before the footbridge, except for 5 m, lie within values calculated using the methodology in the CEN standards, through an analysis of the mean values plus two standard deviations, with the equivalent position after the footbridge. It is clear for positions 2 m and 5 m before the footbridge that the magnitude of the negative pressure peak is larger than after the footbridge; indeed for

position 5 m before the footbridge, the mean plus two standard deviation results are beyond the limits calculated after the footbridge. Considering the peak-to-peak pressure difference for position 5 m indicates a time base of 0.1 seconds, relating to a distance of 7 - 9 m, which as discussed corresponds to the aerodynamically shaped driving carriage nose of Train 1. Therefore the tip of the train nose will be beneath the footbridge as the negative pressure is recorded at the position 5 m before the footbridge and thus the increased magnitude could be due to a confinement of the flow separating from the front of the train. Similar values were also obtained for Train 2 and Train 3. It should be noted that due to the small nature of these differences it is not possible to draw firm conclusions on whether the footbridge has an influence on the aerodynamic flow at this measuring site, but indicates that this would be an interesting topic for further research in the future to assess the influence of confinement on aerodynamic flow development.

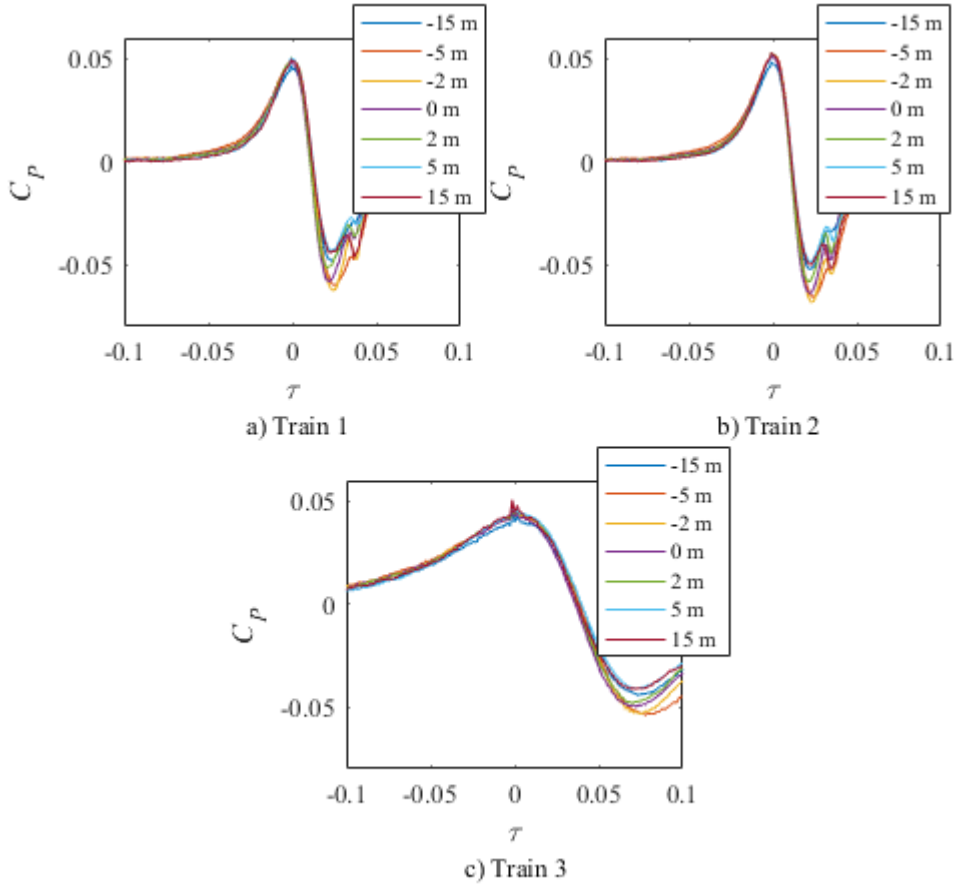

Figure 14: Nose pressure development on the barrier at each measuring position at height 2.5 m for each train analysed.

5.6 Load calculations

The load force on the barrier as a train passes can be estimated by integrating the peak pressure values (found in the nose region) across the height of the barrier. Breaking the barrier into sections centred on the pressure tap measuring position allows the load on a 2.4 m wide section to be calculated. The 2.4 m section was chosen based on the size of each bay between vertical

RSJ beam. The overall load coefficients can be defined as,

$$C_Y = \frac{\sum_i \overline{C_{P_{ij}}} A_{ij} (\mathbf{n}_{ij} \cdot \mathbf{y})}{A_{ref}} \tag{5}$$

where $\overline{C_{P_{ij}}}$ is the ensemble average pressure coefficient for each pressure tapping associated with discretised area A_{ij}. $\mathbf{n}_{ij}$ is the normal unit vector associated with discretised area A_{ij} (directed away from the centre of track), and $\mathbf{y}$ the unit vectors associated with axes Y. The force coefficient can then be used to estimate the actual force applied to the barrier by applying,

$$C_Y = \frac{F_Y}{\frac{1}{2}\rho V_{train}^2 A_{ref}} \tag{6}$$

where F_Y is the lateral force applied to the barrier and A_{ref} is the reference area based on the barrier height and the 2.4 m section over which the force is calculated ($A_{ref} = 10.032$ m^2). It should be noted that due to the measuring positions chosen for each test site that the load calculations could only be made for site 1. As such, in this calculation V_{train} is taken as the maximum train speed through the measuring site (63.33 m/s for Trains 1, 2 and 3 and 33.5 m/s for Train 4). Table 5 presents the peak load coefficient and force values for each train type.

In general, the estimated values of force applied by each type passenger train are very similar, with results lying within the bounds of standard deviation to the ensemble mean. Although the force coefficients for Train 4 are much larger, the actual force applied to the barrier is lower due to the reduced maximum line speed for Train 4. As observed for the pressure coefficient data, results for each measuring position along the acoustic barrier are similar and within bounds of uncertainty; therefore it can be considered that the force is uniform across the barrier.

5.7 Fatigue loading analysis

Every time a train passes the barrier, the transient pressure that is applied to the barrier causes a transient structural loading, which contributes to its fatigue life. When designing trackside infrastructure engineers must consider the magnitude, frequency and number of loads subjected to the barrier over the structure design life span. The results presented show a large spread in the magnitude of pressure values measured on the different acoustic barriers assessed. The differences are mainly due to the distance of the barrier from the centre of track, although the potential interaction between different types of infrastructure such as footbridges was highlighted. The results also indicated a variation in peak pressure magnitudes created by different train types, due to the shape and profile of the different train types which use the railway.

In total, on average 117 trains pass each measuring site on the track nearest to the barrier each day. If only the large peak-to-peak pressures are considered, i.e. around the nose and tail of the train, then there are a total of 234 load cycles induced into the barrier each day. For an average barrier no maintenance period of 20 years this equates to more than 1.5 million load cycles. It should be noted that the results presented in this paper do not consider the rail traffic travelling in the other direction on the other track past the measuring sites. Analysis indicates the key pressure features are also observed for trains travelling on the opposite track but that peak pressure magnitudes are much lower due to the increased distance between the relative centre of track and the barrier. Although the magnitudes are much lower, the number of load cycles experienced by the barrier clearly increases.

Here, an analysis to determine the transient structural loading caused

by different train types passing the barrier is presented. The amount and magnitude of fatigue cycles caused by the transient pressure time histories can be analysed by means of a 'rainflow' counting technique. This technique was first proposed by Tatsuo Endo in 1967 to breakdown any load-time history into its constituent fatigue cycles and their respective range and mean [13]. A fully documented description about the methodology of the rainflow counting analysis is provided in standards such as ASTM E1049-Standard Practices for Cycle Counting in Fatigue Analysis [1].

The rainflow analysis is applied in an attempt to characterise the magnitudes of pressure variation observed by the barrier during the passage of the typical train types examined. To obtain a representative load distribution for each train type, the rainflow analysis was performed on the averaged normalised transient pressure signal of each corresponding train type. The information of this rainflow analysis can be used to perform a fatigue load analysis and therefore to determine the amount of cycles of a certain pressure range/amplitude caused by corresponding train types.

Figure 15 shows the rainflow analysis in the form of a rainflow matrix for the overall action of the maximum pressure change, given as a pressure coefficient C_P. The amplitude determines the range/intensity of the fatigue cycle. The mean determines if the cycle is compressive or tensile and the number of cycles indicates the amount of cycles for the corresponding amplitude and mean. Compressive cycles have a negative mean, whereas tensile cycles are positive. Figure 15 indicates a large quantity of small magnitude variations associated with the highly turbulent flow and as the magnitude of pressure change increases the number of variations decrease. Results indicate that the overall trend is towards negative mean values, essentially acting as a compressive force on the barrier. Figures 15(a) - 15(c) indicate

a similar distribution of pressure magnitudes between Trains 1, 2 and 3, whereas figure 15(d) for Train 4 shows a wide range in cycle type with at low amplitudes but also higher pressure magnitudes than observed for the other trains.

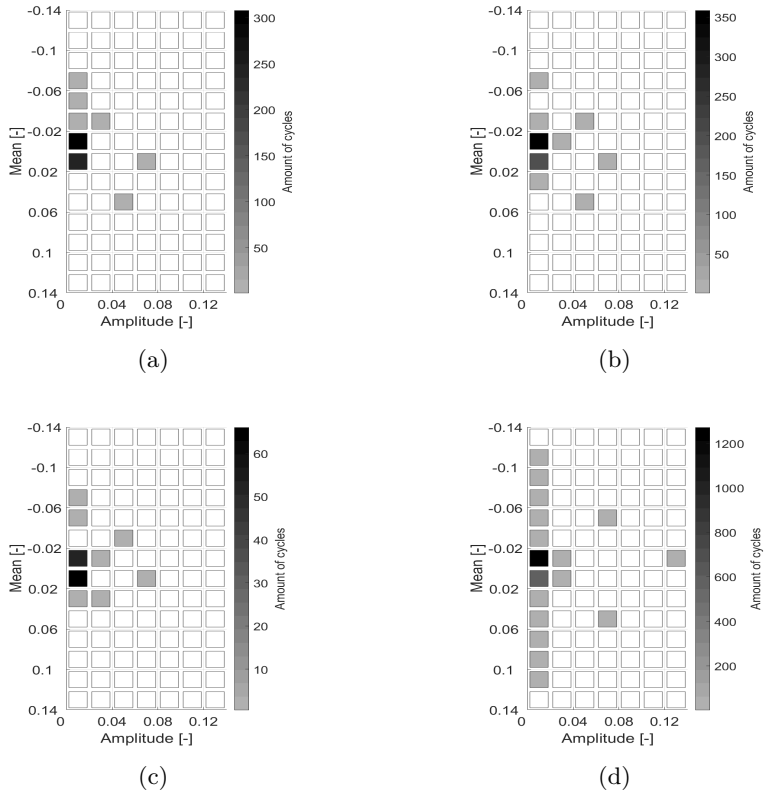

Figure 15: Rainflow matrix for pressures measured on the site 1 acoustic barrier 3.72 m from COT at height 2.5 m for train types (a) Train 1, (b) Train 2 (c) Train 3 and (d) Train 4.

Figure 16 shows the annual accumulated fatigue load caused by different train types at different barrier heights. The assumed amount of trains of the corresponding type passing the barrier on a daily basis is given in table 6. Operational train speeds (also provided in table 6) were used to calculate pressure ranges from the normalised rainflow analysis amplitudes. The most damaging cycles are located at the high amplitude end, due to

the very large ranges. It is typical that the highest numbers of cycles occur at low amplitudes, representing the small fluctuations in the transient pressure signal. For that reason, low amplitudes (regardless of their cycle number) are neglected when fatigue loading is of interest, due to very little contribution to the caused damage. For that reason, only amplitudes where $C_P \geq 0.04$ were taken into account, consequently, bars corresponding to the lowest amplitude range in figure 16 (100 to 150 Nm^2), correspond to normalised amplitudes of $0.04 \leq C_P \leq 0.06$ and so on for higher amplitude bars.

Figure 16 illustrates that Train 4 causes the highest amplitudes of up to 350 Nm^2 (figure 16(b) and 16(c)), however due to only two train passes per day, the amount of cycles of those amplitudes is relatively small. Train 3 contributes the highest amounts of cycles for pressure amplitudes of 100 Nm^2 to 200 Nm^2 at the height 1.5 m and 2.5 m on the barrier (figure 16(b) and 16(c)). This is not too surprising as this type of train passes the barrier the most often over the time scale of one year (table 6). Train 2 causes most of the load cycles in the 200 Nm^2 to 250 Nm^2 range at a height of 1.5 m, whereas Train 1 contributes only a relatively small amount of cycles between 100 Nm^2 to 200 Nm^2. Clearly the largest fluctuations depended on train type and as such load calculations should account for the different types of traffic observed on the railway.

Furthermore, figure 16 shows that the barrier is exposed to largest pressure amplitudes and corresponding cycles at a height of 1.5 m (figure 16(b)). With increasing height, amplitudes and corresponding cycles appear to decrease (figure 16(c) and 16(d)). Results obtained at the lowest measurement position (figure 16(a)) suggest that the barrier at this height is relatively sheltered from the transient pressure load. For that reason, none of the pass-

ing train types contribute to the fatigue load at this measurement height. Only Train 4 exhibits a small contribution for the lowest pressure range (100 Nm^2 to 150 Nm^2); however, again the amount of cycles is relatively small compared to cycles of similar amplitude at higher measurement positions (figure 16(a)).

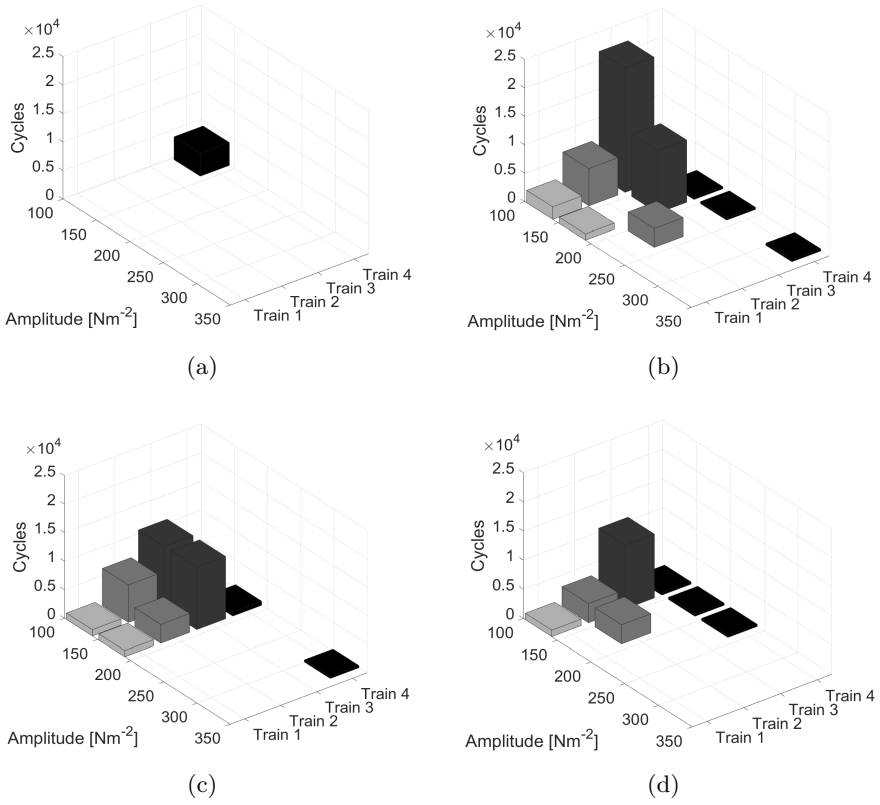

Figure 16: Pressure ranges and corresponding cycles for the site 1 acoustic barrier at 3.72 m from COT measured for different heights on the barrier (a) height 0.5 m, (b) height 1.5 m (c) height 2.5 m and (d) height 3.5 m, for different trains passing the barrier over a year.

6 Conclusions

A detailed series of experiments were conducted to assess the magnitude of pressure loads acting on acoustic barriers located next to a high speed

railway line. The results from measurements made across a number of different sites enabled for the first time an assessment of the influence of barrier distance from centre of track and to assess potential influence from other trackside infrastructure. The results presented indicated a number of important findings:

- The pressure development measured on the acoustic barrier was of the same form as previous studies, with peak magnitudes to similar levels for high speed passenger trains. Peak pressure magnitudes were larger in the bogie and carriage mid-height regions, reducing above the train roof.

- Peak pressure magnitudes were largest around the train nose and tail regions. The Train 3 twelve car set has an additional large peak due to the coupling of two six car sets.

- Comparison of absorptive and reflective type barriers exhibited little difference in pressure development and peak magnitudes.

- As the barrier distance from centre of track is increased the magnitude of pressures measured decreased. Fitting a curve of best fit to the results indicated that the same curve form could be used to estimate both the positive and negative nose pressures.

- Differences in peak pressure magnitudes were observed for results measured underneath the footbridge, suggesting a possible influence of the footbridge on the aerodynamic flow development; however, results were close to within two standard deviations of the ensemble mean.

- The CEN standards methodology provides a good estimation to the pressure coefficient measured on the barrier for most positions anal-

ysed.

- The calculated load across a section of barrier analysed was shown to be uniform along the barrier.
- Analysis of peak pressure magnitudes and the number of train passes across the barrier life span indicated that there are a large quantity of small magnitude pressure changes and a smaller amount of large magnitude changes.
- The barrier is exposed to largest pressure amplitudes and corresponding cycles at a height of 1.5 m, and with increasing height amplitudes and corresponding cycles decrease.
- Large pressure fluctuations depend on train type and as such load calculations should account for the different types of traffic observed on the railway.

Acknowledgements

The authors wish to thank Dr Mingzhe He from the University of Birmingham and Navraj Kallah from UK high speed infrastructure for their help conducting the experiment.

References

[1] ASTM E1049-85(2017) standard practices for cycle counting in fatigue analysis, ASTM international, west conshohocken, pa, 2017, www.astm.org.

[2] Highways agency. environmental barriers: Technical requirements. ha66/95. 1995.

[3] Christopher Baker, Sarah Jordan, Timothy Gilbert, Andrew Quinn, Mark Sterling, Terry Johnson, and John Lane. Transient aerodynamic pressures and forces on trackside and overhead structures due to passing trains. part 1 model scale experiments part 2 standards applications. Proceedings of the Institution of Mechanical Engineers, Part F: Journal of Rail and Rapid Transit, 228:37–70, 2012.

[4] M Belloli, B Pizzigoni, F Ripamonti, and D Rocchi. Fluid–structure interaction between trains and noise-reduction barriers: numerical and experimental analysis. WIT Transactions on the Built Environment, 105:49–60, 2009.

[5] CEN European Standard. EN 1991-2 - Eurocode 1: Actions on structures-Part 2: Traffic loads on bridges, 2003.

[6] CEN European Standard. EN 14067-4 Railway applications - Aerodynamics Part 4: Requirements and test procedures for aerodynamics on open track, 2013.

[7] DB. Ril 804.5501 - noise protection systems at railway lines. Technical report, Deutsche Bahn, 2010.

[8] S. Lachinger, M. Reiterer, and H. Kari. Comparison of calculation methods for aerodynamic impact on noise barriers along high speed rail lines. In World Conference on Railway Research 2016, 2016.

[9] P. Lichtneger and B. Ruck. Full scale experiments on vehicle induced transient pressure loads on roadside walls. Journal of Wind Engineering and Industrial Aerodynamics, 2017.

[10] P Moran and R P Hoxey. A probe for sensing static pressure in two-dimensional flow. Journal of Physics E: Scientific Instruments, 12(8):752, 1979.

[11] A.D. Quinn, C.J. Baker, and N.G. Wright. Wind and vehicle induced forces on flat plates part 1: wind induced force. Journal of Wind Engineering and Industrial Aerodynamics, 89(9):817 – 829, 2001.

[12] A.D. Quinn, C.J. Baker, and N.G. Wright. Wind and vehicle induced forces on flat plates part 2: vehicle induced force. Journal of Wind Engineering and Industrial Aerodynamics, 89(9):831 – 847, 2001.

[13] Darrell Socie. Rainflow cycle counting : A historical perspective. In Y. Murakami, editor, The Rainflow Method in Fatigue, pages 3 – 10. Butterworth-Heinemann, 1992.

[14] Munemasa Tokunaga, Masamichi Sogabe, Tetsuo Santo, and Kiyoshi Ono. Dynamic response evaluation of tall noise barrier on high speed railway structures. Journal of Sound and Vibration, 366:293 – 308, 2016.

[15] Dalei Wang, Benjin Wang, and Airong Chen. Vehicle-induced aerodynamic loads on highway sound barriers part 2: numerical and theoretical investigation. Wind and Structure, 17(5):479–494, 2013.

[16] Dalei Wang, Benjin Wang, and Airong Chen. Vehicle-induced aerodynamic loads on highway sound barriers part1: field experiment. Wind and Structures, 17(4):435–449, 2013.

	Train 1			Train 2			Train 3			Train 4		
Absorptive	C_Y	F_Y (N)	SD (N)	C_Y	F_Y (N)	SD (N)	C_Y	F_Y (N)	SD (N)	C_Y	F_Y (N)	SD (N)
Maximum	0.087	2141	220	0.088	2166	231	0.081	1997	218	0.12	987	61
Minimum	-0.064	-1574	200	-0.072	-1783	198	-0.068	-1665	170	-0.12	-996	42
Reflective												
Maximum	0.071	1751	92	0.075	1846	89	0.073	1742	108	0.132	1086	114
Minimum	-0.068	-1682	128	-0.074	-1815	121	-0.075	-1857	119	-0.122	-1001	327

Table 5: Estimation of lateral load coefficients and the lateral force subjected to the site 1 barrier in the absorptive and reflective configuration for each type of train analysed.

Train type	Assumed passings per day	Assumed train speed (m/s)
Train 1	6	63.33
Train 2	18	63.33
Train 3	60	63.33
Train 4	2	44.4

Table 6: Amount and operational velocities of corresponding train types passing the barrier daily.